crystals

MDPI

Article

Microwave Bow-Tie Diodes on Bases of 2D Semiconductor Structures

Steponas Ašmontas [1], Maksimas Anbinderis [1,2], Aurimas Čerškus [1,2], Jonas Gradauskas [1,2], Andžej Lučun [1] and Algirdas Sužiedėlis [1,*]

[1] Laboratory of Electron Processes, Center for Physical Sciences and Technology, Saulėtekio Ave. 3, 10257 Vilnius, Lithuania; steponas.asmontas@ftmc.lt (S.A.); maksimas.anbinderis@ftmc.lt (M.A.); aurimas.cerskus@ftmc.lt (A.Č.); jonas.gradauskas@ftmc.lt (J.G.); andzej.lucun@ftmc.lt (A.L.)
[2] Department of Physics, Vilnius Gediminas Technical University, Saulėtekio Ave. 11, 10223 Vilnius, Lithuania
* Correspondence: algirdas.suziedelis@ftmc.lt; Tel.: +370-5-2124539

Abstract: Planar microwave bow-tie diodes on bases of selectively doped semiconductor structures are successfully used in the detection and imaging of electromagnetic radiation in millimeter and submillimeter wavelength ranges. Although the signal formation mechanism in these high-frequency diodes is said to be based on charge-carrier heating in a semiconductor in a strong electric field, the nature of the electrical signal across the bow-tie diodes is not yet properly identified. In this research paper, we present a comprehensive study of a series of various planar bow-tie diodes, starting with a simple asymmetrically shaped submicrometer-thick *n*-GaAs layer and finishing with bow-tie diodes based on selectively doped GaAs/AlGaAs structures of different electrical conductivity. The planar bow-tie diodes were fabricated on two different types of high-resistivity substrates: bulky semi-insulating GaAs substrate and elastic dielectric polyimide film of micrometer thickness. The microwave diodes were investigated using DC and high-frequency probe stations, which allowed us to examine a sufficient number of diodes and collect a large amount of data to perform a statistical analysis of the electrical parameters of these diodes. The use of probe stations made it possible to analyze the properties of the bow-tie diodes and clarify the nature of the detected voltage in the dark and under white-light illumination. The investigation revealed that the properties of various bow-tie diodes are largely determined by the energy states residing in semiconductor bulk, surface, and interfaces. It is most likely that these energy states are responsible for the slow relaxation processes observed in the studied bow-tie diodes.

Keywords: selectively doped semiconductor structure; microwave bow-tie diode; semi-insulating substrate; polyimide substrate

check for updates

Citation: Ašmontas, S.; Anbinderis, M.; Čerškus, A.; Gradauskas, J.; Lučun, A.; Sužiedėlis, A. Microwave Bow-Tie Diodes on Bases of 2D Semiconductor Structures. *Crystals* **2024**, *14*, 720. https://doi.org/10.3390/cryst14080720

Academic Editor: Lin Gan

Received: 28 June 2024
Revised: 31 July 2024
Accepted: 9 August 2024
Published: 11 August 2024

Copyright: © 2024 by the authors. Licensee MDPI, Basel, Switzerland. This article is an open access article distributed under the terms and conditions of the Creative Commons Attribution (CC BY) license (https://creativecommons.org/licenses/by/4.0/).

1. Introduction

Six decades have passed since the International Conference on the Physics of Semiconductors, which took place at the University of Exeter and where microwave radiation was introduced as a possibility to heat the charge carriers in a semiconductor [1]. This technique represented a reliable tool for investigating hot carrier phenomena in strong electric fields because the carrier-heating circuit became galvanically isolated from the signal-registering circuit. These investigations brought into practice the term "electromotive force of hot carriers", which promoted applied research into the phenomenon [2]. A new sort of microwave detector, the so-called "hot-carrier microwave detector", presenting typical linear I-V characteristics was identified [2]. The active region of the detector was an ohmic point contact of micrometer dimensions, positioned on the surface of a semiconductor crystal (Ge, Si, and InSb), with another ohmic contact of a large area on the opposite side of the crystal. The hot-carrier detectors were characterized by high voltage sensitivity that was close to the sensitivity of the Schottky diodes at that time (of the order of tens of millivolts per microwatt). In addition to high sensitivity, the diodes were characterized by high burn-out

power and high electrical stability over a long period of use. The obstacle to the practical application of these detectors was the unreliable design of the whisker-point contact and the high series resistance of the diodes (tens of kOhms). Two decades later, a new design of hot-carrier detector, the so-called "bigradient diode", was proposed [3]. The electric field in this asymmetrically shaped homogeneous semiconductor structure has different gradients, from the point where the electric field strength is maximal to the ends of the bigradient diode. The separation of charge carriers occurs in the homogeneous semiconductor, due to the different electric field gradients, and, as a result, an asymmetry of electrical conduction and bigradient electromotive force arises in the barrier-less semiconductor structure. The phenomenon of I-V asymmetry and electromotive force in a homogeneous asymmetrically shaped semiconductor was recognized as the first discovery from Lithuania in 1977, and this discovery was only the 185th during the half-century of the existence of the USSR [3]. The original bigradient diodes suffered from low voltage sensitivity and high electrical resistance. However, these disadvantages did not prevent them from being used in the detection of high-power electromagnetic radiation. Another advantage of the bigradient diode is the possibility of detecting electromagnetic radiation in the THz frequency range because the cut-off frequency of this diode is determined by the electron momentum relaxation time [3]. Modified versions of bigradient diodes with reduced electrical resistance allowed for using the diodes in the detection of electromagnetic radiation in the GHz-THz range [4]. The resistance of the diodes was reduced by the heavier doping of the more narrowed side of the diodes, thereby introducing an n-n^+ junction into the bigradient diode, which was renamed to an asymmetric bow-tie diode. These bow-tie diodes were successfully used for THz imaging [5–8], and their voltage sensitivity was raised using partial gating of the two-dimensional electron gas channel [9,10]. A decrease in the electrical resistance of the bow-tie diode was achieved by doping the narrower part of the diode; however, in this case, the metal contact reached the narrowest part of the diode in terms of micrometric dimension. The detected voltage of the modified bigradient diode became strongly dependent on the quality of the ohmic contacts of the diode, and this inevitably increased the influence of the contacts of the diode on the detected voltage. Two voltages, bigradient electromagnetic force (EMF) and the one detected on the contacts, had opposite polarities. Therefore, the resultant voltage was lower than expected or had even changed polarity. Specifically, the polarity of the detected voltage of the asymmetrically shaped bow-tie n-Si and n-GaAs [5] diode corresponded to the polarity of the electromotive force of hot electrons across the n-n^+ junction. However, the use of selectively doped semiconductor structures in the bow-tie diodes brings an additional degree of freedom for the ambiguity seen in the origin of the total voltage. For example, there are no data about the polarity of the voltage detected across the terminals of InGaAs-based bow-tie diodes [5,8,11].

In this research, we present a comprehensive study of various planar bow-tie diodes, starting with a simple asymmetrically shaped n-GaAs layer of submicrometer thickness, and finishing with bow-tie diodes on a base of selectively doped GaAs/AlGaAs structures of different electrical conductivity. The diodes were positioned on two types of substrates: a bulky semi-insulating GaAs substrate and an elastic dielectric polyimide film of micrometric thickness. The microwave diodes were investigated using both DC and high-frequency probe stations, which allowed us to examine a large number of diodes and collect a large amount of data for statistical analysis of the electrical parameters of different diodes. In addition, the use of the probe stations simplified the possibility of comparing the properties of the bow-tie diodes in the dark and under the white light of a microscope lamp; this way, they enabled clarification of the nature of the voltage detected by the diodes.

2. Samples and Methods

Constructively, two types of diodes have been developed: bow-tie diodes on a crystal substrate and bow-tie diodes on a polyimide dielectric film. Hereafter, we will refer to them as crystal and filmy diodes, correspondingly. Schematic views of crystal and filmy bow-tie diodes of asymmetric configuration are presented in Figure 1. During the manufacturing

process, the crystal diodes were produced first. However, since the lateral dimensions of the diode were comparable to the vertical dimensions of the semiconductor substrate, a technical problem arose that was related to the cutting of the diode matrix situated on the crystal substrate into individual crystal diodes and to their subsequent installation into waveguides for conducting microwave experiments. Another circumstance leading to the choice of the filmy diode design was associated with the high-frequency experiments being conducted: shunting the microwave currents via the semiconductor substrate weakened the microwave currents flowing through the bow-tie diode and, thus, reduced the voltage-power sensitivity of the diodes.

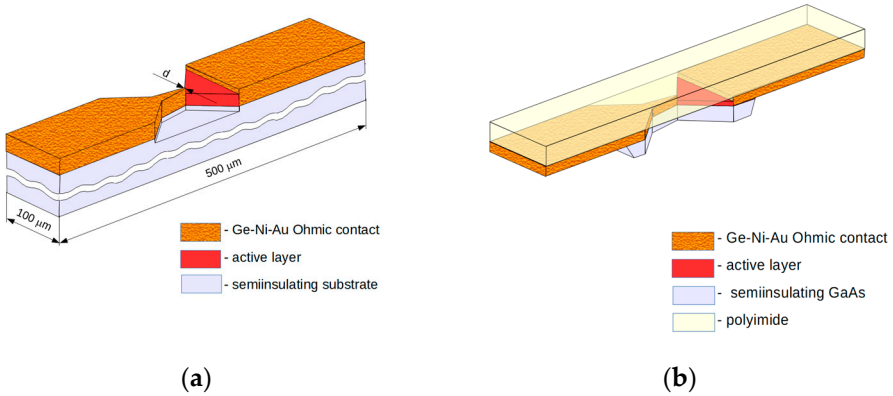


Figure 1. Schematic view of bow-tie diodes of asymmetric configuration: (**a**) crystal diode; (**b**) filmy diode.

Two types of topologically different bow-tie diodes were fabricated and investigated: asymmetric diodes (AD) and symmetric diodes (SD). A schematic view of the diodes is shown in Figure 2. The width d of the narrowest part of the diodes was 1, 2, and 3 μm.

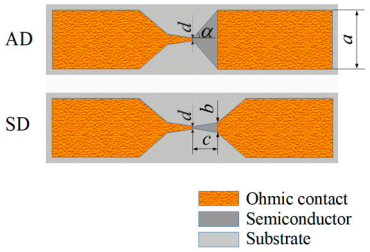


Figure 2. Schematic view of asymmetric (AD) and symmetric (SD) bow-tie diodes.

Five types of thin semiconductor layers were used for the fabrication of the bow-tie diodes:

1. A heavily doped thick *n*-GaAs layer of submicrometric dimensions, epitaxially grown onto a non-intentionally doped *i*-GaAs layer. Hereafter, we will refer to it as the TG structure.
2. A selectively doped GaAs/AlGaAs structure without a spacer (SDWS structure).
3. A selectively doped GaAs/AlGaAs structure with a thick spacer (SDTS structure).
4. A selectively doped GaAs/AlGaAs structure with a homogeneously doped barrier (SDHD structure).
5. A selectively doped GaAs/AlGaAs structure with a delta-doped barrier (SDDD structure).

Cross-section views of the investigated structures and their energy band diagrams, including electron density distribution, are shown in Figure 3.

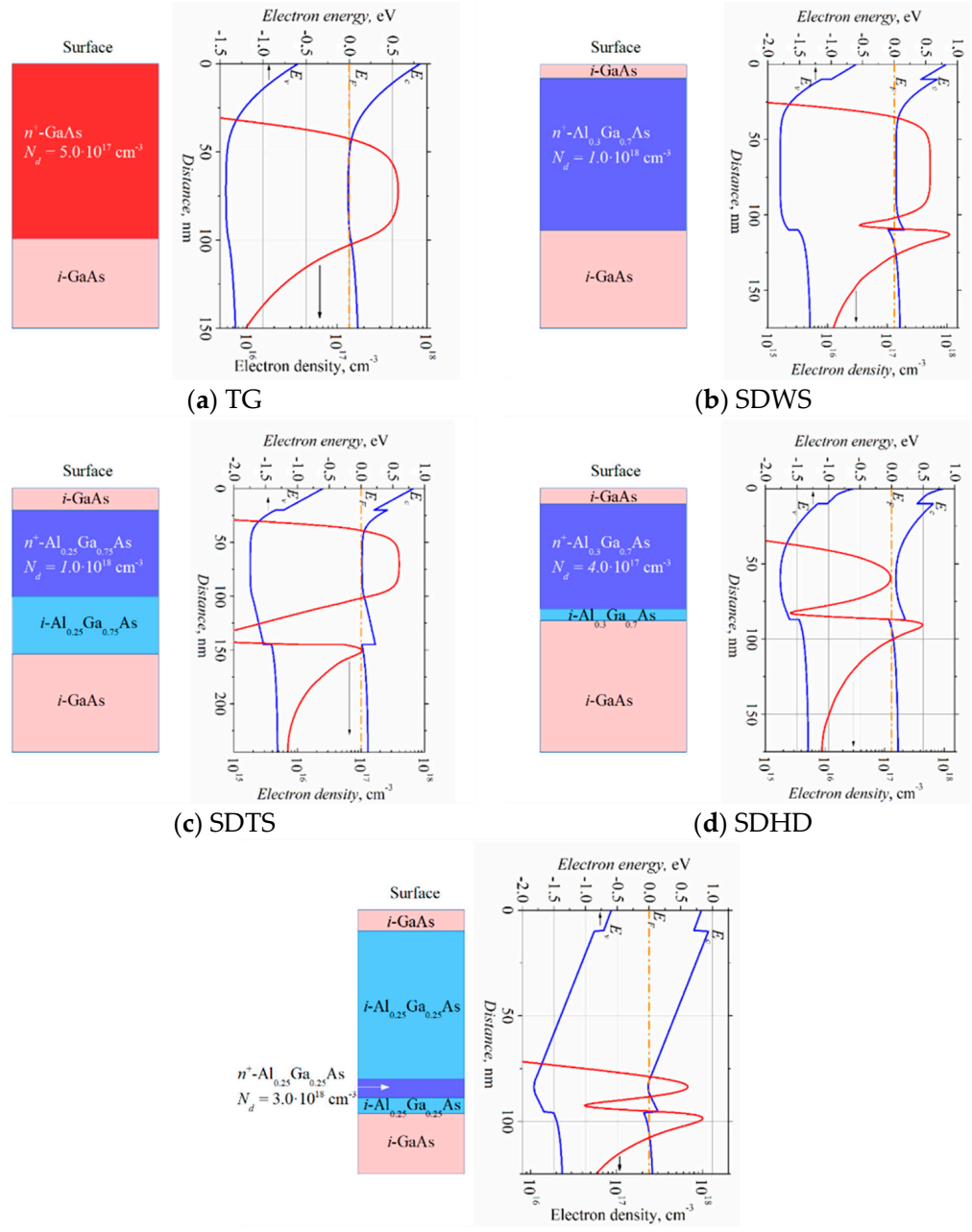


Figure 3. Cross-section of the investigated semiconductor structures and their energy band diagrams, showing the electron density distribution: (**a**) a heavily doped thick *n*-GaAs layer of submicrometric dimension epitaxially grown onto a non-intentionally doped *i*-GaAs layer (TG structure); (**b**) a selectively doped GaAs/AlGaAs structure without a spacer (SDWS structure); (**c**) a selectively doped GaAs/AlGaAs structure with a thick spacer (SDTS structure); (**d**) a selectively doped GaAs/AlGaAs structure with a homogeneously doped barrier (SDHD structure); (**e**) a selectively doped GaAs/AlGaAs structure with a delta-doped barrier (SDDD structure).

All these structures are actually the selectively doped ones, except for the TG structure, in which the electrical current flows through a heavily doped GaAs layer of submicrometer thickness. The selectively doped structures differ from each other in terms of the characteristics of the spacer layer. The SDWS has no spacer, the SDTS has a thick spacer, and the other two structures differ in the barrier doping method: the entire barrier of the SDHD is homogeneously doped, and the SDDD has a delta-doped barrier.

The detailed technology used in the fabrication of both crystal and filmy bow-tie diodes has been described in [12]. The general sequence of processes was as follows. First of all, the crystal diodes were produced. Then, the plate with the crystal diode matrix was divided into two parts; the first was used to measure the parameters of the diodes on the crystal substrate, and the second was used to proceed with the technological operations of transferring the bow-tie diodes onto the polyimide film. A 100-nanometer etching depth was chosen to ensure the necessary confinement of the conductive channels in the semiconductor structures (see the cross-sections of the structures in Figure 3). The specific contact resistance and the sheet resistance of the conductive layer were measured using the classical so-called transfer length model (otherwise known as the transmission line model) when electrical resistance is measured between differently spaced ohmic contacts on a rectangular semiconductor mesa [13]. All the measurements of electrical parameters of the bow-tie diodes and test structures were performed using DC and high-frequency probe stations, which ensured obtaining a sufficiently large number of electrical parameters for statistical processing of the measured data. Using the probe stations also allowed us to perform the on-wafer experiments in darkness and under illumination with white light. The electrical parameters of the produced semiconductor structures are presented in Table 1. An example of contact resistivity and the sheet resistance evaluation is presented in Appendix A.

Table 1. Sheet resistance R_{sh}, low-field electron mobility μ_0, electron sheet density n_s, and contact resistivity ρ_c of the investigated semiconductor structures in the dark and under illumination with white light.

Structure	$R_{sh\text{-}ill}$, Ω/□	$R_{sh\text{-}drk}$, Ω/□	μ_0, cm^2/(V·s)	$\rho_{c\text{-}ill}$, Ω·mm	$\rho_{c\text{-}drk}$, Ω·mm	$R_{sh\text{-}drk}/R_{sh\text{-}ill}$	$n_{s\text{-}drk}$, cm^{-2}
TG	590 ± 4	680 ± 8	3000	0.14 ± 0.05	0.15 ± 0.07	1.15	3×10^{12}
SDWS	880 ± 2	930 ± 2	5400	0.29 ± 0.06	0.29 ± 0.06	1.06	1.2×10^{12}
SDTS	1320 ± 30	1380 ± 35	2400	0.34 ± 0.11	0.53 ± 0.13	1.05	1.9×10^{12}
SDHD	1750 ± 8	2110 ± 10	4800	0.73 ± 0.20	0.79 ± 0.27	1.21	0.6×10^{12}
SDDD	910 ± 4	960 ± 6	5500	0.21 ± 0.16	0.19 ± 0.06	1.05	1.2×10^{12}

The TG structures had the highest electrical conductivity, and the selectively doped SDHD structure with a homogeneously doped barrier had the lowest conductivity. The contact resistivity correlated with the sheet resistance values: the higher the sheet resistance, the higher the contact resistivity. The TG and SDHD structures were most sensitive to illumination: their sheet resistance decreased by about 15%, while the decrease in the sheet resistance was only 5% for other structures. It should be noted that the spread of sheet resistance values reached up to several percent, while the spread of contact resistivity values was within 15–75%. The scattering of the sheet resistance and contact resistivity values was random and did not depend on illumination, in terms of whether the samples were in the dark or illuminated.

The current–voltage (*I*-*V*) characteristics were measured using the Süss MicroTec probe station EP6 with DC probes (FormFactor, Inc., Livermore, CA, USA) and Agilent E5270B precision measurement equipment (Agilent Technologies, Inc., Santa Clara, CA, USA). The voltage–power (*V*-*P*) characteristics of the diodes were measured in the K_a frequency range using a Cascade Microtech (FormFactor, Inc., Livermore, CA, USA) high-frequency probe station, while ACP40-A-GS-250 probes were used to connect the diodes to the measurement station. An SHF BT45 broadband bias tee separated the detected DC voltage signal from the microwave signal. The microwave diodes were illuminated with the Eiko EKE21V150W photo-lamp (color temperature 3240 K) at the maximum illuminance of 14,000 lx. The spectral characteristics of the photo-lamp are presented in Appendix B.

Photoluminescence studies of these structures were performed using continuous wave photoluminescence (CWPL) and time-resolved photoluminescence (TRPL) techniques. The CWPL spectra were measured using a standard photoluminescence setup with a fully automated focal length monochromator of 1 m. An Ar-ion laser was used as the excitation source, with photon energy in the range of 2.2–2.7 eV. The output power was set to reach an intensity of 1.36 W/cm^2. The CWPL was detected by a thermoelectrically cooled GaAs photomultiplier operating in the photon-counting regime. The TRPL measurements were performed using a pulsed 531 nm (photon energy 2.3 eV) DPSS microchip laser with an FWHM pulse of 400 ps. The pulse repetition rate was 10 kHz, and the average output power was set to 0.4 mW (0.018 W/cm^2). The transient PL was measured with a time-correlated single-photon counting (TCSPC) system at peak maximum.

The voltage sensitivity S, low-field electrical resistance R_0, the asymmetry of the *I-V* characteristic, and the coefficient of nonlinearity of the *I-V* characteristic β of the diodes were investigated. The voltage sensitivity at a 30 GHz frequency was calculated from the slope of the *V-P* characteristic in its linear region. The low-field electrical resistance of the diodes was derived from their *I-V* characteristics at zero applied voltage U. The asymmetry of the *I-V* characteristic of a semiconductor structure containing an n-n^+ junction with perfect ohmic contacts is directly related to the voltage sensitivity S of the microwave diode, presuming that the relaxation of the average energy of hot electrons can be neglected [3]:

$$S = \frac{R_r - R_f}{2U} \tag{1}$$

where R_r and R_f stand for the electrical resistance of the diode, measured at reverse and forward voltage U, respectively. This way, it is possible to predict the voltage sensitivity of the hot-electron detector from its *I-V* characteristic if it is assumed that all the microwave radiation falling on the diode is absorbed. Another parameter characterizing the heating of electrons in an electric field is β, the nonlinearity coefficient of the *I-V* characteristic. In the so-called warm electron region, the current density j flowing through a semiconductor can be approximated by the square dependence on the electric field strength E [14]:

$$j = \sigma_0\left(1 + \beta E^2\right)E, \tag{2}$$

where σ_0 marks the low-field electrical conductivity.

3. Results

This section presents the statistically processed results of the electrical parameters of the bow-tie diodes, such as voltage sensitivity, low-field electrical resistance, the asymmetry of the *I-V* characteristic, and the coefficient of nonlinearity of the *I-V* characteristic. All the parameters were measured and calculated for about 20 diodes of each type in the dark and under illumination with white light. Finally, we present the results of the photoluminescence study of the investigated structures, which provide information about charge transfer in selectively doped semiconductor structures.

3.1. Voltage Sensitivity

The median values of voltage sensitivity of the bow-tie diodes in the dark and under illumination are presented in Figure 4. Asymmetrically and symmetrically shaped bow-tie diodes are denoted as AD and SD, respectively.

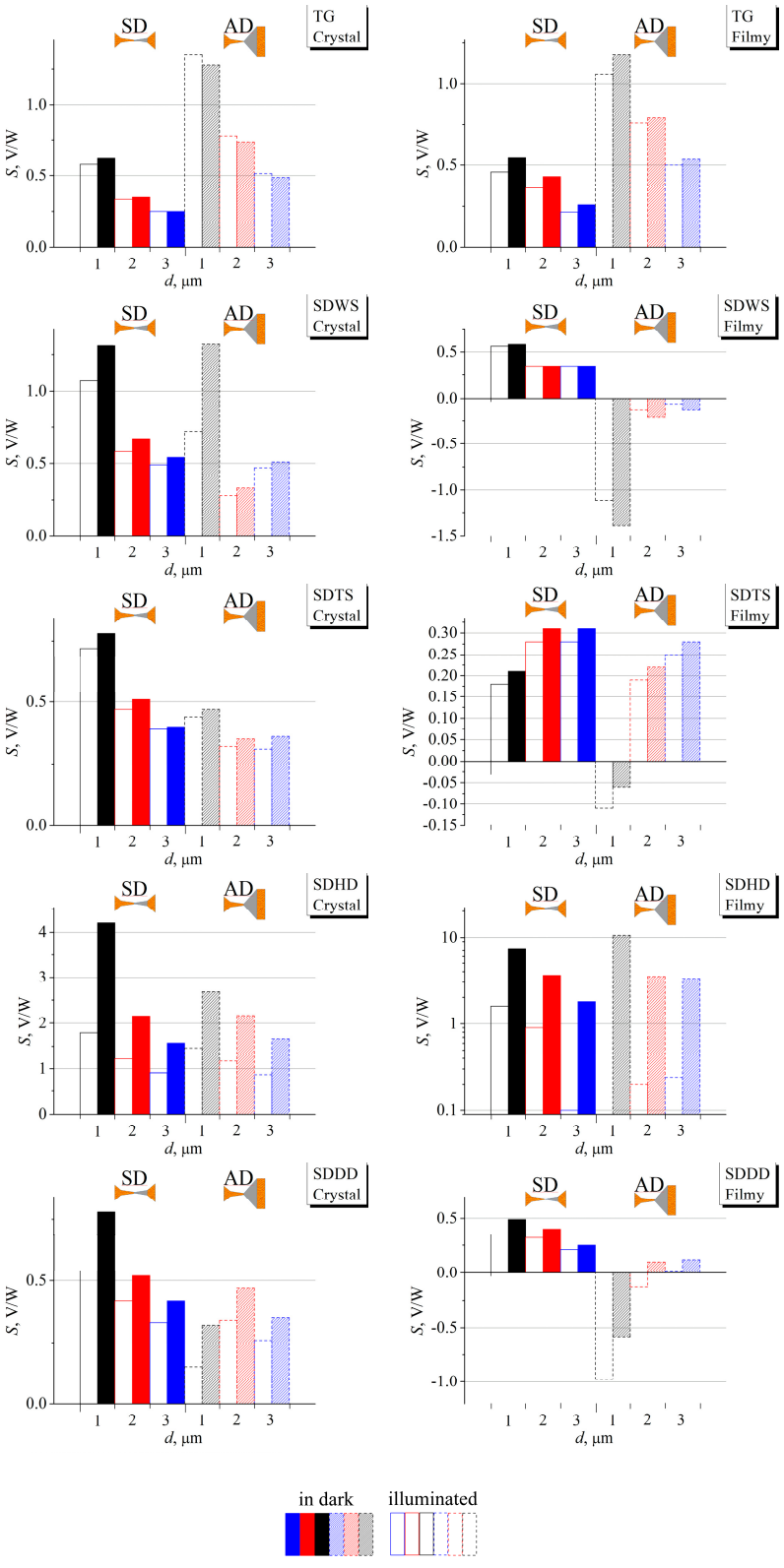


Figure 4. Statistical representation of the voltage sensitivity of various bow-tie diodes in the illuminated and unilluminated scenarios. SD and AD denote symmetric and asymmetric bow-tie diodes, respectively, with *d* indicating the width of the diode's narrowest part in micrometers. Positive values of *S* correspond to the polarity of the thermal electromotive force of hot electrons.

The voltage sensitivity of the asymmetrically shaped bow-tie diodes, i.e., the ratio of the detected voltage U_d to the incident microwave power P_i, can be expressed as [10]:

$$S = \frac{U_d}{P_i} = \frac{2R_{sh}\mu_0 \tan\alpha}{3d^2 \ln\frac{a}{d}} \frac{P}{P_i} N, \quad (3)$$

where α, a, d are the widening angle of the active part of the diode and the widths in the widest and narrowest parts of the diode, respectively (see Figure 2); P denotes the microwave power absorbed by the diode; N stands for the factor that depends on microwave frequency, electron momentum, and energy relaxation times and the Maxwell relaxation time. An analogous expression can be applied to the symmetrically shaped bow-tie diodes by changing a to b (see Figure 2). As follows from Equation (3), the voltage sensitivity of the diode with d =1 μm should be 7 or 8 times higher than that of the diode with d = 3 μm, and 3.5 ÷ 4 times higher than that of the diode with d = 2 μm. In reality, these ratios should be lower, because this estimation does not take into account the fact that part of the microwave radiation absorbed by the diode decreases with the higher electrical resistance resulting from its narrower geometry. Therefore, the experimental results presented in Figure 4 show a weaker dependence of the voltage sensitivity on the width of the diode's neck d. The qualitative dependence of voltage sensitivity on d is observed for the symmetrical diodes of all the studied semiconductor structures, while in the case of the asymmetrical diodes, this is only true for the TG, SDTS, and SDHD structures. Illumination does not significantly affect the sensitivity of the bow-tie diodes on a crystal substrate, but it has an impact on the sensitivity of the diodes, based on the SDHD structure and partially on the AD1 and SD1 diodes on the base of the SDWS structure.

The situation changes in the case of the diodes on polyimide film. Only filmy bow-tie diodes on the TG and partially on the SDHD structures, both asymmetric and symmetric, are characterized by voltage sensitivity that increases with width d. Furthermore, in the case of the SDWS structure, the polarity of the voltage detected on asymmetric bow-tie diodes is opposite to that of the symmetric diodes, both in the dark and under illumination. The voltage sensitivity of the filmy diodes on the bases of the SDTS and SDDD structures decreases with wider d and even changes its polarity in the case of the AD1 diodes. Only filmy diodes on the bases of the TG and SDHD structures have a slight preference against their counterparts on the crystal substrate in terms of voltage sensitivity. Illumination slightly reduces voltage sensitivity for most diodes. However, the voltage sensitivity of the bow-tie diodes based on SDHD structures decreases, and this decrease is more fully expressed in the case of filmy diodes.

3.2. Low-Field Electrical Resistance

The low-field electrical resistance R_0 of the bow-tie diode consists of the geometric R_g [15] and parasitic contact resistance R_c of the diode:

$$R_0 = R_g + R_c = \frac{R_{sh}}{2\tan\alpha} \ln\frac{a}{d} + \frac{\rho_c}{d} \quad (4)$$

where ρ_c represents the contact resistivity. An analogous expression is used to calculate the electrical resistance of the symmetrically shaped bow-tie diodes, but the width a is replaced by the width b in Equation (4) (see Figure 2). A statistical representation of the low-field electrical resistance of the bow-tie diodes is depicted in Figure 5. The theoretical values of the electrical resistance, calculated using Equation (4), are represented by the short dotted lines in Figure 5.

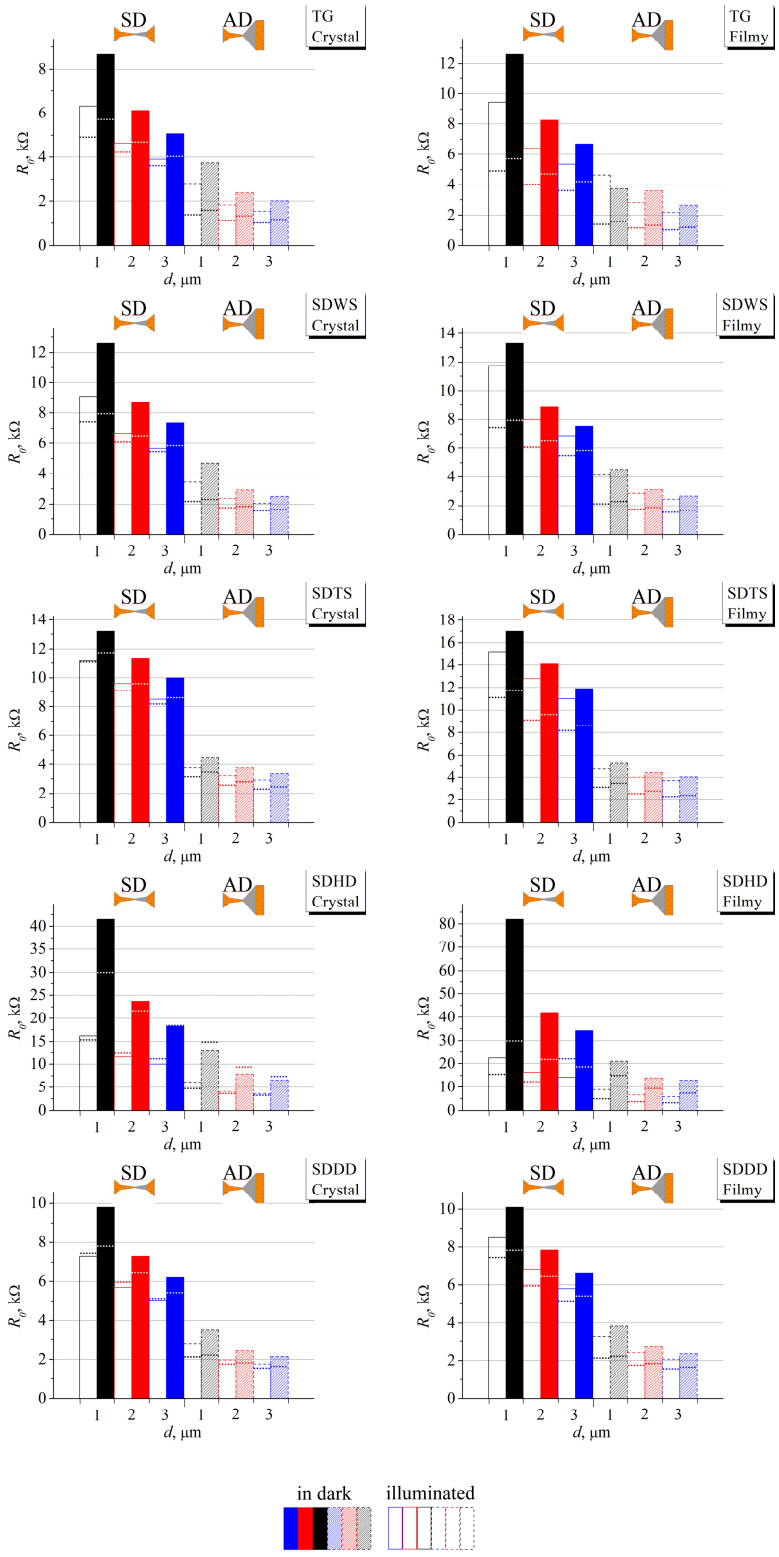


Figure 5. Statistical representation of the low-field electrical resistance of the bow-tie diodes in the dark and under illumination. SD and AD denote symmetric and asymmetric bow-tie diodes, with *d* indicating the width of the diode's narrowest part in micrometers. The short dotted lines show the theoretical values calculated using Equation (4).

Before discussing the statistical results of the electrical resistance, it is necessary to note the different scattering of the measured results for individual structures.

The percentage standard deviation of the measured results was in the order of several percent for the TG, SDTS, and SDDD structures, while it reached tens and up to 100 percent in the case of the SDWS and SDHD structures. Illumination had a marked influence on the dispersion of the resistance values for diodes based on SDHD structures as compared to that of the TG structure diodes, while the scattering of the electrical resistance of the diodes on the bases of SDWS, SDTS, and SDDD structures weakly depended on illumination. No well-defined systematic dependence of resistance dispersion on the neck width d was observed.

The measured electrical resistance values were higher than the ones calculated according to Equation (4) for most of the diodes. The only exceptions were the illuminated bow-tie diodes on the crystal substrate based on SDHD and SDDD structures, which showed experimental resistance values lower than the theoretical values. However, this small difference was within the permitted errors of measurement. The difference between the experimental and theoretical resistance values was significantly bigger for the filmy diodes and for the asymmetrically shaped diodes, except for the bow-tie diodes on the base of the SDHD structure: the difference between the experimental and theoretical values was large in the case of symmetrically shaped diodes.

An ambiguous dependence of the illumination-caused resistance change was observed. The reaction of the diodes to the illumination was, on average, the same for both crystal and filmy diodes. The resistance of both symmetrically and asymmetrically shaped bow-tie diodes (both crystal and filmy) slightly decreased under illumination. However, the symmetrically shaped bow-tie diodes were more sensitive to illumination than the asymmetrically shaped ones. The smallest light-induced decrease in the electrical resistance was demonstrated by the bow-tie diodes on the base of the SDTS structure. The bow-tie diodes on the base of the SDHD structure were the most light-sensitive. A different reaction to the illumination was observed in the case of the bow-tie diodes based on the SDHD, compared to the TG, SDDD, SDWS, and SDTS structures (the structures are listed in the order of light-sensitivity decrease). Namely, the electrical resistance of the SDHD bow-tie diodes on the polyimide film changed to a greater extent compared to that of the diodes on the crystal substrate. The electrical resistance of the symmetrically shaped bow-tie diodes on the same base as the SDHD structure was more sensitive to illumination than that of their asymmetrically shaped counterparts. This is especially noticeable for the diodes on polyimide film. The electrical resistance of the bow-tie diode on the base of the SDHD structure became more responsive to illumination as the neck width d narrowed. The electrical resistance of the symmetrically shaped bow-tie diodes with d = 1 μm on the base of the SDHD structure was 60% more sensitive to illumination compared to the diodes with d = 3 μm. This finding, to a lesser extent, also applies to the other diodes: this difference reached approximately 20% for the bow-tie diodes on the base of the SDDD structure and reached less than 5% for the bow-tie diodes on the bases of other structures.

Comparing the low-field electrical resistances of the crystal and filmy bow-tie diodes, the average ratio of the resistances of the diodes on polyimide and crystal substrates showed that the lowest ratio was exhibited by the SDWS structures, while the highest ratio was exhibited by the SDHD structures. Table 2 presents the average ratios of the electrical resistance of the diodes on the polyimide film and crystal substrate for all the studied structures.

Table 2. The average ratios of the electrical resistance of the diodes on the polyimide film and crystal substrate, based on all the studied structures.

Structure	TG	SDWS	SDTS	SDHD	SDDD
$R_{0\ filmy}/R_{0\ crystal}$	1.54	1.12	1.26	1.66	1.13

3.3. Asymmetry of I-V Characteristics

The asymmetry of the *I-V* characteristic of an asymmetrically shaped planar semiconductor structure with an n-n^+ junction can be expressed in terms of the geometrical and electrical parameters of the less-doped n-type region. The difference in electrical resistance, ΔR, of the planar bow-tie diode with perfect ohmic contacts, recorded as the voltage U across the n-n^+ junction is applied in both the reverse and forward directions, is expressed as follows [12]:

$$\Delta R = R_r - R_f = \frac{4UR_{sh}\tan\alpha[(1+s)\tau_E + \tau_M]}{3d^2 \ln\frac{a}{d}}, \quad (5)$$

where τ_E marks the electron energy relaxation time, τ_M is the Maxwell relaxation time in the n-region of the n-n^+ junction, and s stands for the exponent in the dependence of electron momentum relaxation time on electron energy; a, d and α denote the geometrical parameters of the bow-tie diode (see Figure 2). Thus, the prospective voltage sensitivity of bow-tie diodes can be evaluated from their *I-V* characteristic, according to Equation (1). Therefore, we introduce a term to represent the asymmetry of the *I-V* characteristic, which we will denote as AsIV:

$$AsIV = \frac{\Delta R}{2U} \quad (6)$$

Table 3 presents the data of the *I-V* asymmetry values of the bow-tie diodes with a 1 μm-wide neck, calculated according to Equation (5).

Table 3. The values of the *I-V* asymmetry of the bow-tie diodes with the neck dimension d = 1 μm, calculated according to Equation (5), when the diodes were in the dark and under illumination. AD and SD mean the asymmetric and symmetric bow-tie diode configuration, respectively.

Structure	$\frac{\Delta R}{2U}$, arb. u.			
	AD		SD	
	Illuminated	Dark	Illuminated	Dark
TG	90	110	25	28
SDWS	140	150	37	39
SDTS	210	220	55	58
SDHD	280	400	74	105
SDDD	140	150	38	40

A statistical representation of the measured asymmetry of the *I-V* characteristic of the investigated bow-tie diodes is shown in Figure 6.

The first thing that stands out when looking at Figure 6 is the large variation in the *I-V* asymmetry values. Secondly, in the dark scenario, the sign of the *I-V* asymmetry for almost all bow-tie diodes is opposite to what would be expected for the *I-V* characteristic of a structure with an n-n^+ junction. The same sign of this asymmetry is also typical of the illuminated bow-tie filmy diodes that are based on SDTS and SDHD structures. Qualitatively, the experimental values of the *I-V* asymmetry correlate with the theoretical values, presented in Table 3, when the AD and SD diodes (both crystal and filmy) based on TG and SDWS structures were illuminated. The same correlation is also observed for the illuminated crystal SD diodes on the base of the SDTS structure and for the illuminated filmy SD diodes on the base of the SDDD structure. Only the filmy bow-tie diodes that were based on the SDHD structure demonstrated an asymmetry polarity coinciding with the *I-V* asymmetry sign of the semiconductor n-n^+ structure in the dark. However, in the case of SD diodes, the order of the *I-V* asymmetry values is close to the theoretical value, while in the case of the AD diodes, the measured *I-V* asymmetry exceeds the calculated value by two orders of magnitude.

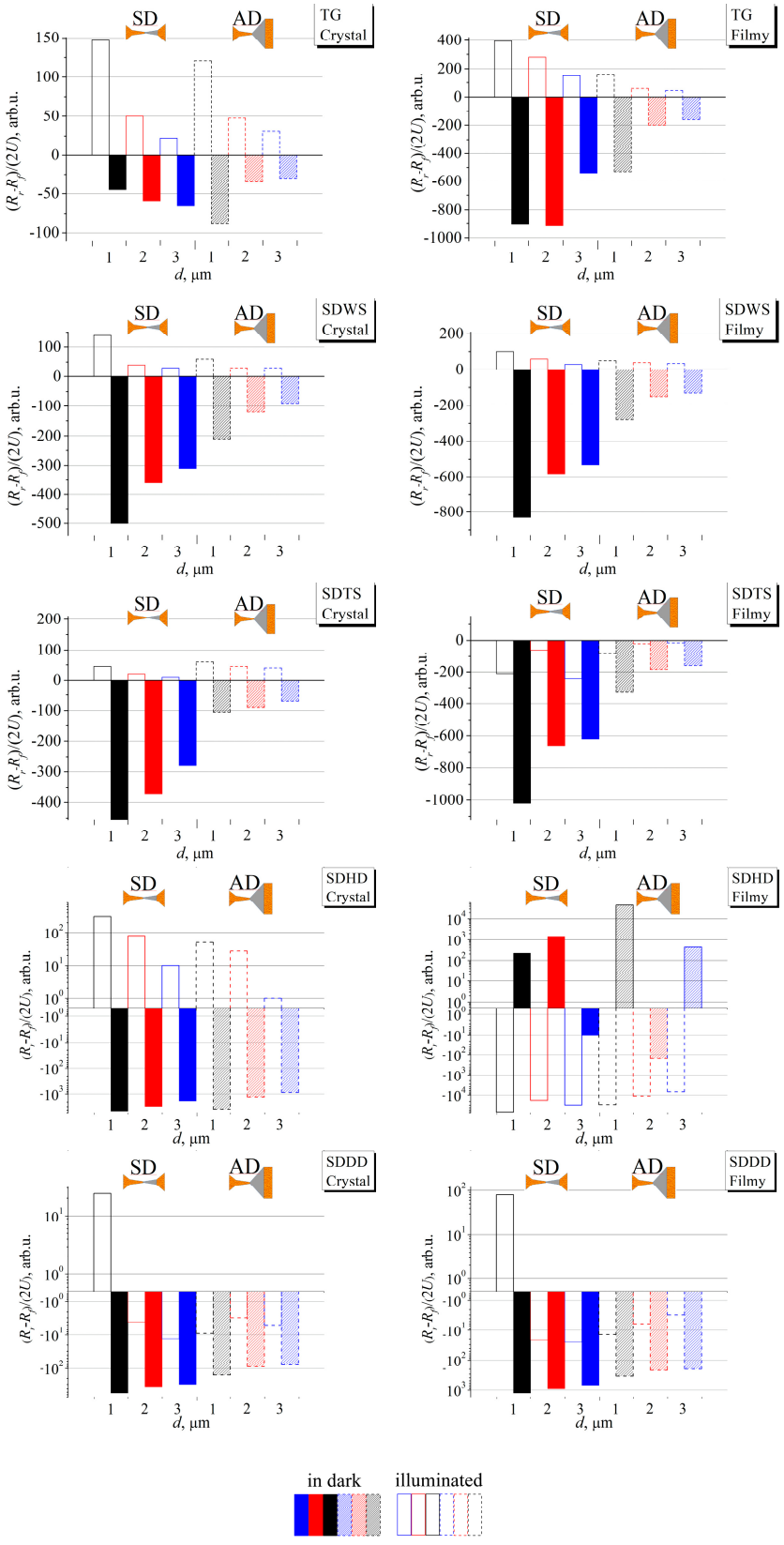


Figure 6. Statistical data of the asymmetry of *I-V* characteristic of various bow-tie diodes, both illuminated and in the dark. SD and AD denote the bow-tie diodes, with *d* indicating the width of the neck in micrometers.

3.4. Nonlinearity Coefficient of the I-V Characteristic

The presented conflicting results of the asymmetry of the *I-V* characteristic force us to delve into the reasons for this inconsistency between the theory and the experiment. Therefore, before proceeding to a discussion of the obtained results, we examine the *I-V* characteristics of the bow-tie diodes at higher values of the applied voltage U. The nonlinearity factor β of an *I-V* characteristic describes the deviation of a device's *I-V* characteristic from the linearity at high U values.

If voltage U is applied across the contacts of the asymmetrical bow-tie diode, then, assuming that the electrons are heated in the maximum electric field E and using Equation (2), the strength of the current flowing through the diode can be expressed as:

$$I = \frac{2Uen_0\mu_0 h \mathrm{tn}\alpha\left(1-\beta E^2\right)}{\ln\frac{a}{d}} = \frac{2Uen_0\mu_0 h \mathrm{tn}\alpha\left[1-\beta\left(\frac{2U\mathrm{tn}\alpha}{d\ln\frac{a}{d}}\right)^2\right]}{\ln\frac{a}{d}} \tag{7}$$

where e is the electron charge, n_0 and μ_0 denote the electron density and mobility at zero electric field strength, and h stands for the thickness of the electrically conductive layer of the bow-tie diode. Other geometrical parameters of the bow-tie diode, a, d, and α, are explained in Figure 2. The negative sign preceding the non-linearity coefficient β is based on the fact that in general, the electron mobility decreases with increasing electric field in a semiconductor. An analogous expression of the current strength in the symmetrically shaped bow-tie diode can be used by substituting a with b in Equation (7). From Equation (7), the electric field strength in the narrowest part of the n-region of the bow-tie diode is expressed as follows:

$$E = \frac{2U\mathrm{tn}\alpha}{d\ln\frac{a}{d}} \tag{8}$$

Assuming that the electrons moving through a bow-tie diode are heated up in a strong electric field that is concentrated in the narrowest part of the n-region of the diode, and, as a result, that electron mobility decreases and the current I gets weaker, we can approximate I using Equation (7). The variable parameters of the approximation are the thickness of the conducting layer of the diode h and the coefficient of nonlinearity β of the *I-V* characteristic. The approximation was performed within the applied voltage U ranging from −1V to +1V. According to Equation (8), the maximum electric field strength E in an asymmetrically narrowed bow-tie diode where d = 1 µm reaches ~ 5 kV/cm for the limiting values of U. The approximated *I-V* curves of the crystal bow-tie diodes on the base of the SDHD structure are shown in Figure A3 of Appendix C. This approximation was performed for the *I-V* characteristics of both dark and illuminated diodes.

The obtained values of the non-linearity coefficient of all the investigated bow-tie diodes are presented in Figure 7.

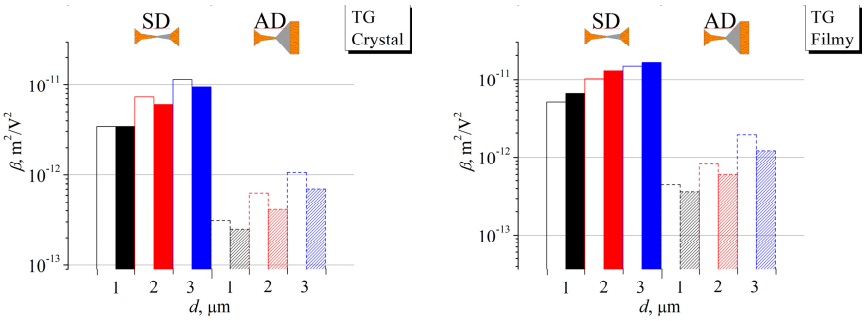


Figure 7. *Cont.*

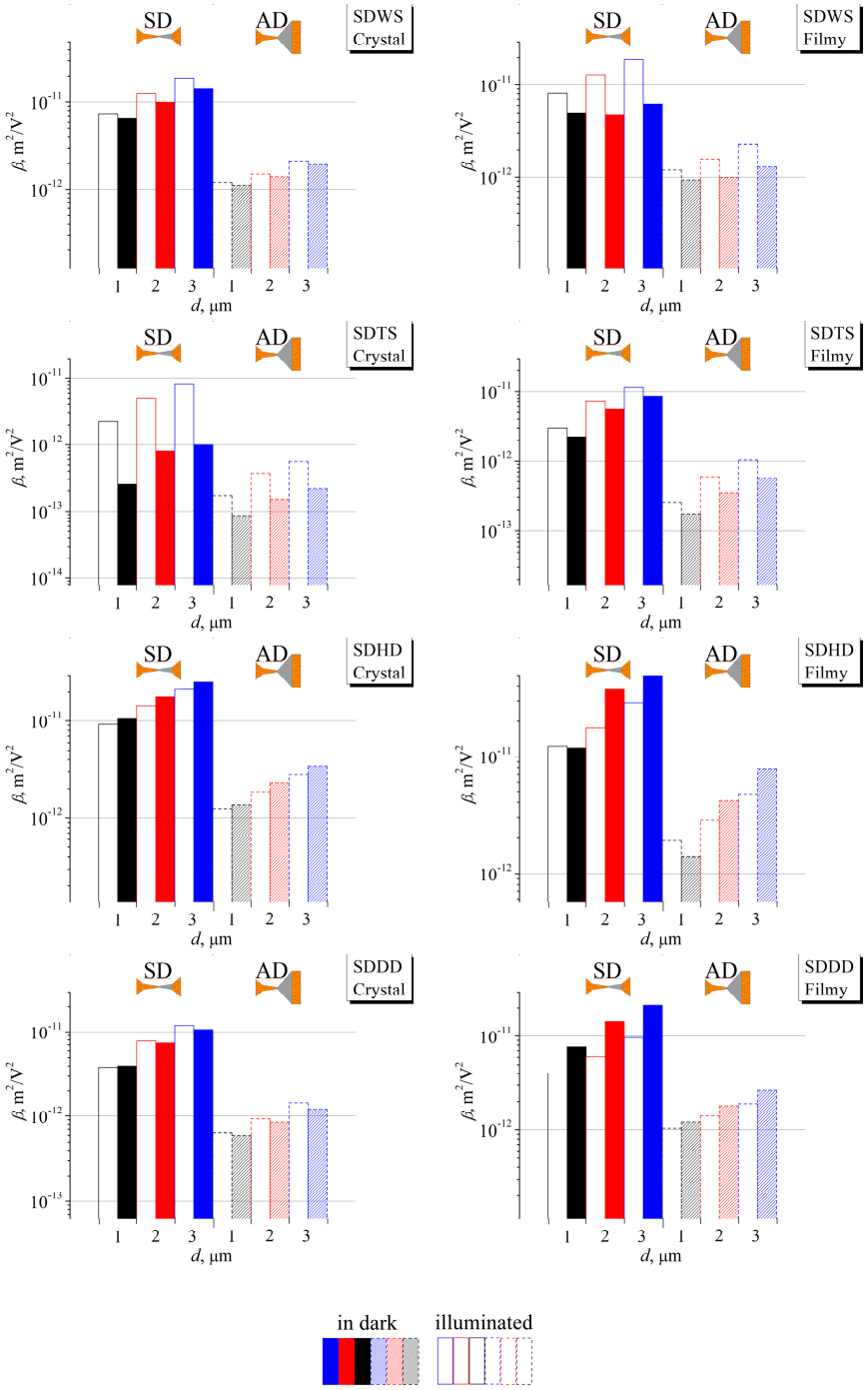


Figure 7. Statistical representation of the non-linearity coefficient of the *I-V* characteristics of various bow-tie diodes, both illuminated and in the dark. SD and AD denote the bow-tie diodes, with the corresponding width of the neck *d* in micrometers.

A common observation across all the studied structures is that the values of the nonlinearity coefficient increase as the neck width *d* of the bow-tie diodes increases. Additionally, the nonlinearity coefficient of symmetric bow-tie diodes is significantly higher than that of asymmetric ones. This would imply that electron heating decreases as the electric field in the narrowest part of the bow-tie diode increases, which is impossible. The experimental results indicate that the strength of the current flowing through the bow-tie diode does not decrease due to a reduction in electron mobility in a strong electric field. Instead, it likely decreases due to the "stealing" of electrons as they travel through the diode. This raises a natural question: where does this occur? The most likely location for this "action"

would be the neck of the bow-tie diodes, the narrowest point through which electrons pass. However, this assumption is contradicted by the fact that the current deviates more from the linear dependence on the voltage as the neck width d increases. Therefore, we performed additional *I-V* measurements on the test samples of the studied structures to assess their conductivity and the quality of their ohmic contacts. The test structure was a mesa with a width of 100 μm, featuring ohmic contacts separated by various distances L: 10, 20, 30, 40, 60, and 100 μm. The electrical current strength I flowing through the mesa of the test structure between two contacts separated by distance L is expressed as:

$$I = \frac{ehwUn_0\mu_0}{L}\left[1 - \beta\left(\frac{U}{L}\right)^2\right] \quad (9)$$

where w is the width of the mesa.

The dependencies of the approximated non-linearity coefficient β of the *I-V* characteristics of the test structures on the distance L between the ohmic contacts, both in dark conditions and under illumination, are presented in Figure 8. It is evident that the nonlinearity coefficient increases with the distance L between the ohmic contacts. This is similar to the situation with bow-tie diodes, where the strength of the current flowing through the sample depends on its geometry. In this case, however, the deviation from the linear *I-V* characteristic is greater when the electrons travel a longer path L. Also, the nonlinearity coefficient is higher for the bow-tie diodes with a wider neck. In both cases—when the distance between the contacts increases and when the width of the conducting layer increases—the electric field strength in the samples decreases. The different response of the crystal SDTS-based bow-tie diode test structures to light is worth noting. For the bow-tie diodes, the nonlinearity coefficient under illumination was significantly higher than in the dark (approximately 8 times greater for SD diodes and 3 times greater for AD diodes). However, for the test structures, this ratio did not exceed 1.5. The nonlinearity coefficient of the test structures and bow-tie diodes on the bases of other semiconductor structures was even less sensitive to light: the ratio of the nonlinearity coefficient of the crystal bow-tie diodes when they were illuminated and in the dark varied between 1.0 and 1.5 in the case of the TG, SDWS, and SDDD structures. The nonlinearity coefficient of the crystal bow-tie diodes on the base of the SDHD structure was a little bit higher in the dark than under illumination. For the crystal bow-tie diodes, the discussed ratio of β coefficients under the light and in the dark was almost independent of the neck width d and was within the permitted errors of measurement. The maximum ratio of beta coefficients of "dark" and illuminated diodes reached $2 \div 3$ for the test TG and SDWS structures with L = 100 μm gap, while for the other investigated structures, this maximal ratio did not exceed 1.5. Another noteworthy feature of the SDTS test structures is that for small gap widths L, the nonlinearity coefficient is higher in the light than in the dark. Conversely, when the gap between the contacts exceeds L = 40 μm, the β value in the dark exceeds that under illumination. The relative value of the beta coefficient with respect to its value at maximum electric field strength, $\beta(L)/\beta(10\ \mu m)$, strongly depends on the gap width L between the contacts of the test structures, as illustrated in Figure 8b.

Regarding the behavior of measured nonlinearity coefficients for filmy bow-tie diodes, only those based on the TG structure are qualitatively and quantitatively similar to their crystal counterparts, as shown in Figure 7. For filmy bow-tie diodes based on the SDWS structure, a decrease in β is observed when they are in the dark, whereas for diodes based on the SDHD and SDDD structures, β increases in the dark compared to crystal diodes. Filmy bow-tie diodes based on the SDTS structure exhibit a different behavior: their coefficient of *I-V* nonlinearity shows less dependence on illumination compared to the crystal diodes. (See Appendix D Figure A4).

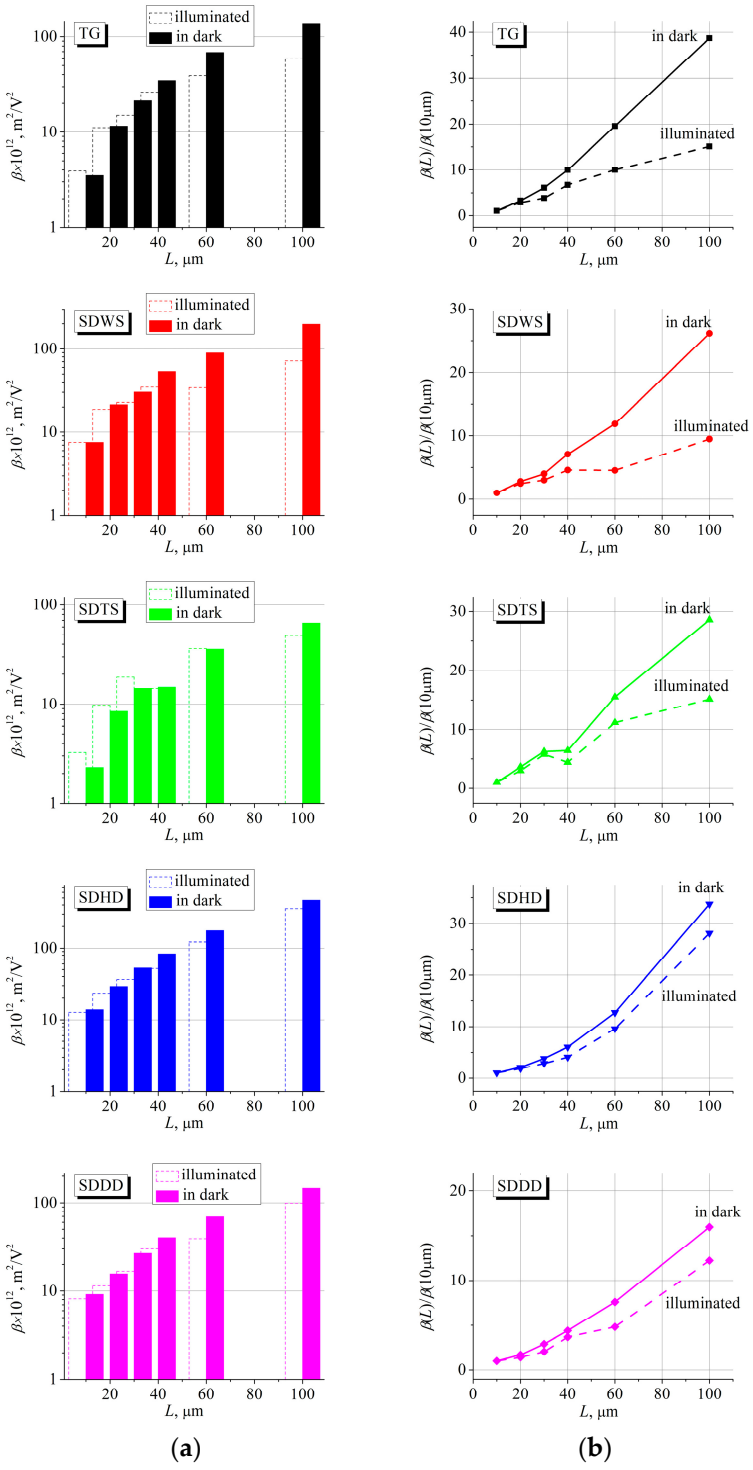


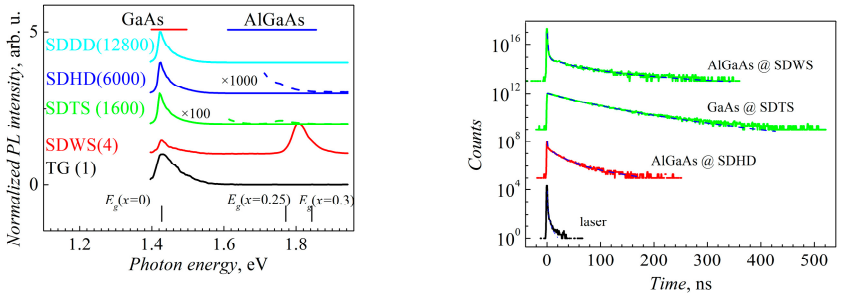
Figure 8. Dependences of the nonlinearity coefficient β of the *I-V* characteristic of test structures on distance L between the ohmic contacts when the structures were in the dark and when they were illuminated: (**a**) histograms of β versus L; (**b**) the dependence of the ratio $\beta(L)/\beta(10\ \mu m)$ on L.

3.5. Photoluminescence Study of the Investigated Structures

The normalized and shifted vertically continuous wave photoluminescence (CWPL) spectra of the structures at room temperature are shown in Figure 9a. One can mark two ranges of the spectra, related, respectively, to the GaAs and AlGaAs layers. The PL band from GaAs is related to recombination from the conduction band to the valence band. The transitions from AlGaAs are associated with the recombination from the conduction

band to the valence band and from free electrons to acceptors. The weakest emission was observed from the TG structure. Emissions that were four times more intense for the main peak of AlGaAs and the weaker peak of GaAs were observed for the SDWS structure. The numbers in parentheses next to the names in Figure 1a and the second column in Table 1 show the ratio between the main PL peaks of the samples and the peak of the TG sample. However, the transient PL of all peaks of both these structures followed the laser pulse (see Table 4). This could be explained by the strong non-radiative recombination at room temperature in these samples. Much more intense photoluminescence was observed from the SDTS, SDHD, and SDDD structures within the GaAs-attributed range. These peaks also showed longer decay times (see Table 4, Figure 9b). The decay times were extracted using the single or double DHARA function or Becquerel decay function in the following form [16]:

$$I(t) = \sum_{i=1}^{2} \alpha_i \left(1 + \frac{c_i t}{\tau_{0i}}\right)^{-\frac{1}{c_i}} \quad (10)$$



(**a**) (**b**)

Figure 9. Photoluminescence spectra of the investigated structures at room temperature: (**a**) normalized CWPL spectra. The numbers in parentheses next to the spectra show the ratio between the main PL peaks of the samples and the peak of the TG sample.; (**b**) TRPL spectra. The spectra are shifted vertically for clarity.

Table 4. The ratio between the main PL peaks of the samples, the fitting results of the TRPL spectra, and the calculated average lifetime and average decay time.

Sample	PL Ratio	τ_{01}, ns	c_1	τ_{02}, ns	c_2	$<\tau>$, ns
laser		0.214	0.420	-	-	0.368
GaAs @ TG	×1			as laser line		
GaAs @ SDWS				as laser line		
AlGaAs @ SDWS	×4			as laser line		
GaAs @ SDTS	×1600	34.9	0.133	-	-	40.3
AlGaAs @ SDTS		0.214	0.420	22.3	0.472	0.781
GaAs @ SDHD	×6000	14.6	0.245	-	-	19.3
AlGaAs @ SDHD		0.214	0.420	10.4	0.345	5.14
GaAs @ SDDD	×12,800	15.6	0.335	-	-	23.5

where τ_{0i} is the lifetime, c_i is the dimensionless parameter, and the parameter α_i satisfies the condition $\sum_i \alpha_i = 1$.

The average lifetime $<\tau>$ is calculated using the following formula [17]:

$$\langle \tau \rangle = \sum_i \frac{\alpha_i \tau_{0i}}{1 - c_i}. \quad (11)$$

A longer average lifetime indicates the better quality of the GaAs layers. Very weak photoluminescence from AlGaAs was detected in the SDTS and SDHD structures. The

AlGaAs region-attributed PL transient form of these samples is composed of two parts. The faster part follows the laser pulse; therefore, it was approximated with the fitting parameters of the laser pulse. The slower part was approximated with the second DHARA function (see Table 4, Figure 9b).

4. Discussion

The voltage sensitivity of the tested bow-tie diodes did not match the sensitivity that was calculated using Equation (3). This discrepancy suggests that the diodes did not have ideal ohmic contacts. The experimentally measured electrical resistance values were higher than those calculated using Equation (4), supporting this observation. However, as shown in Table 1, the contact resistivity values were not critically high and did not significantly impact the experimental resistance values of the bow-tie diodes. For the crystal bow-tie diodes, there was a qualitative and quantitative correlation between the voltage sensitivity and the SD diode neck's width d. In contrast, this correlation was absent in the sensitivity of AD diodes. In the case of filmy diodes, a quantitative and qualitative correlation between the voltage sensitivity and the neck's width was only observed for the bow-tie diodes based on TG structures and partially for those based on SDHD structures. Notably, the TG bow-tie diodes exhibited the lowest contact resistivity, while SDHD diodes had the highest contact resistivity (see Table 2). Moreover, the theoretical electrical resistance values of TG diodes differed from the experimentally measured resistances more than those of SDWS bow-tie diodes (see Figure 5). Additionally, the sign of the detected voltage in SDWS filmy AD diodes was opposite to the sign of the thermoelectric electromotive force of hot electrons (see Figure 4). Therefore, it is unlikely that the discrepancy between the voltage sensitivity of bow-tie diodes and the calculated sensitivity can be attributed solely to the influence of parasitic contact resistance. Furthermore, as demonstrated in the case of a Schottky point contact with a high-resistivity semiconductor [3], the voltage detected across the metal–semiconductor junction was significantly lower than the thermo-EMF of hot carriers detected within the semiconductor. Another possible explanation for the inversion of the detected voltage could be the photogradient phenomenon of hot electrons mentioned in [15]. However, this phenomenon should also affect bow-tie diodes based on other structures, yet it was experimentally observed only in SDWS and partially in SDTS and SDDD Filmy diodes. The influence of the photogradient EMF on the detected voltage is determined by the dependence of electron and hole mobility on the electric field strength in the semiconductor material [3]. However, since the dependence of the mobility of charge carriers on the electric field strength in the studied structures should not differ significantly, the conditions for the appearance of the photogradient EMF in the bow-tie diodes should be similar. Additionally, the polarity of the voltage detected in the dark was inverted for the SDWS bow-tie filmy diodes, and this fact cannot be attributed to photogradient phenomena. As mentioned in the previous section, the asymmetry of the *I-V* characteristic of bow-tie diodes with ideal ohmic contacts should reflect their potential to detect microwave radiation. However, the large variability in the experimental values of this *I-V* characteristic (see Figure 6) and the weak correlation with the experimental voltage sensitivity values (only the asymmetry of some SDHD filmy diodes both qualitatively and quantitatively matched the asymmetry expected in an ideal bow-tie diode) suggest that additional factors are influencing the electrical characteristics of the bow-tie diodes.

By default, when examining the flow of electric current in a bow-tie diode and the voltage detected after exposing the diode to microwave radiation, we assumed that the electron density would remain constant during these processes. However, the experimental results suggest that the electron density actually changes. The higher experimental electrical resistances, compared to the calculated values, indicate a decrease in electron density. This decrease is further evidenced by the sublinear part of the *I-V* characteristics of bow-tie diodes in stronger electric fields. Approximating these characteristics using Equation (7) revealed that the saturation of the electric current in strong electric fields cannot be explained solely by the heating of electrons in the electric field. Instead, the

decrease in electron density as the electrons move through the semiconductor structure must also be considered. The measurements of the nonlinearity coefficient β of the bow-tie diodes and the *I-V* characteristics of the test structures (see Figures 7 and 8) showed that the coefficient depends on the geometry of the sample. Specifically, the nonlinearity coefficient increases with the widening of the diode's neck and is larger in symmetrically shaped bow-tie diodes compared to asymmetrically shaped ones. Additionally, in the test structures, the β value increased as the distance L between the contacts increased. These results indicate that electrons are captured more effectively as they move through the wider neck of the bow-tie diode and when they are more highly concentrated in symmetrically shaped diodes. Furthermore, as electrons travel a longer distance in the test structures, they are more efficiently removed from the charge transfer process. It remains to be determined where the electrons are being captured. Examining the structure of the investigated samples (see Figure 1), we observe that all structures, except for the TG structure, are selectively doped and are composed of combinations of GaAs and AlGaAs layers. The TG structure consists of both intentionally and unintentionally doped GaAs layers. Therefore, in this structure, electrons can be trapped in the bulk of the intentionally doped layer and in the side surfaces of the mesa structure. In contrast, the other investigated structures have additional trapping sites, including the doped AlGaAs layer and the interfaces between the GaAs and AlGaAs layers. Notably, the SDWS and SDHD structures feature a barrier layer made of a ternary $Al_xGa_{1-x}As$ compound with an AlAs mole fraction of x = 0.3. It is well known that the DX centers in $Al_xGa_{1-x}As$ act as efficient electron capture centers when the AlAs fraction exceeds 0.2 [18]. Weak photoluminescence from the AlGaAs layer in the SDTS and SDHD structures further indicates efficient electron capture, which shortens their lifetime (see Figure 9a and Table 4).

In summary, the detected voltage in most of the bow-tie diodes studied in this work is primarily due to the heating of electrons in the microwave electric field. As the DC measurements indicated, the possible capture of electrons in the trapping centers has a greater impact on the electrical resistance of the bow-tie diodes and a weaker effect on the magnitude and polarity of the detected voltage.

5. Conclusions

Detailed studies of bow-tie diodes based on various semiconductor structures designed for microwave radiation detection have led to the following conclusions:

- The polarity of voltage detected in most of the tested bow-tie diodes corresponds to the polarity of the thermoelectric EMF of hot electrons in the semiconductor n-n^+ structure.
- The experimentally measured electrical resistance of the studied microwave diodes exceeds their calculated geometrical resistance; we associate this discrepancy with electron trapping phenomena in semiconductor structures.
- Measurements of the asymmetry and nonlinearity of the *I-V* characteristics of the bow-tie diodes confirmed the fact of electron capture at the surface and interfacial capture centers.
- The transfer of the crystal bow-tie diode onto a polyimide substrate affects the diode's parameters, with the extent of influence varying depending on the diode's structure: the polyimide substrate had a minimal impact on diodes based on the heavily doped thick n-GaAs layer grown on the *i*-GaAs layer and had the greatest impact on bow-tie diodes based on selectively doped structures.

Author Contributions: Conceptualization, A.S. and S.A.; methodology, A.S., S.A. and J.G.; simulations, A.S. and A.L.; microwave investigation A.S., M.A. and A.L.; photoluminescence investigations—A.Č.; writing—original draft preparation, A.S.; writing—review and editing, S.A. and J.G.; visualization, A.S., A.Č. and J.G.; supervision, A.S.; project administration, S.A. All authors have read and agreed to the published version of the manuscript.

Funding: This research received no external funding.

Data Availability Statement: The original contributions presented in the study are included in the article; further inquiries can be directed to the corresponding authors.

Acknowledgments: The authors acknowledge Hadas Shtrikman and Vladimir Umansky from the Braun Center for Submicron Research at the Weizmann Institute of Science, Rehovot, Israel for the MBE-grown structures that were used for sample preparation.

Conflicts of Interest: The authors declare no conflicts of interest.

Appendix A

Approximation of the linear dependence of the electrical resistance of the test structure on the different distances between contacts in the transfer length model for the SDHD structure, which allows us to evaluate the contact resistivity ρ_c of the contacts and sheet resistance R_{sh} of an investigated semiconductor layer.

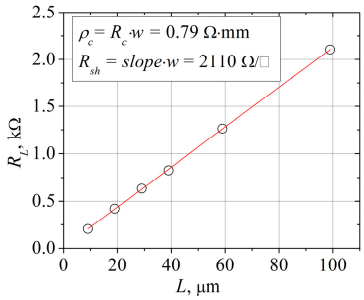


Figure A1. The dependence of the electrical resistance between ohmic contacts of the TLM test structure on the distance between the contacts L (dots). The red line marks the linear approximation of the experimental points; R_c denotes the contact resistance of the contacts, which forms half of the segment cut by the approximate line on the ordinate axis from 0 to the intersection with this axis; w = 100 μm is the width of the mesa of the test structure.

Appendix B

Spectrum of the photo-lamp Eiko EKE21V150W.

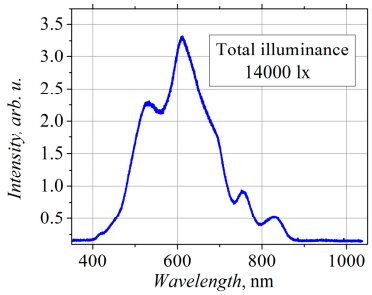


Figure A2. Spectrum of the photo-lamp.

Appendix C

Approximation of the I-V characteristic of the crystal bow-tie diode on the base of the SDHD structure.

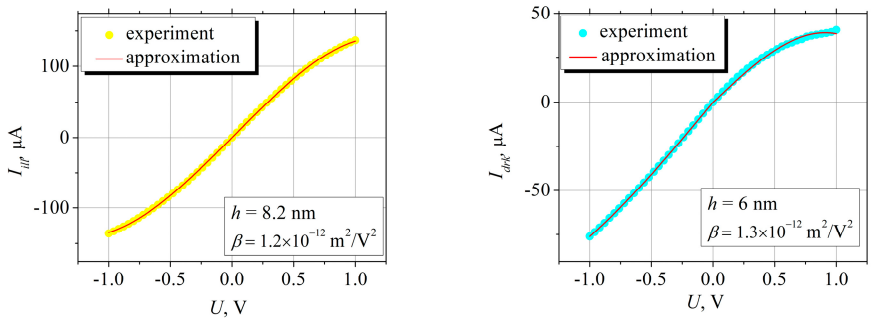


Figure A3. Approximation of the current strength in the crystal AD1 bow-tie diode on the base of the SDHD structure, using Equation (7): (**a**) under illumination; (**b**) in the dark.

Appendix D

The I-V characteristics of the crystalline asymmetrically shaped bow-tie diodes of all the studied structures and the dependencies of the resistance of the diodes on the applied voltage.

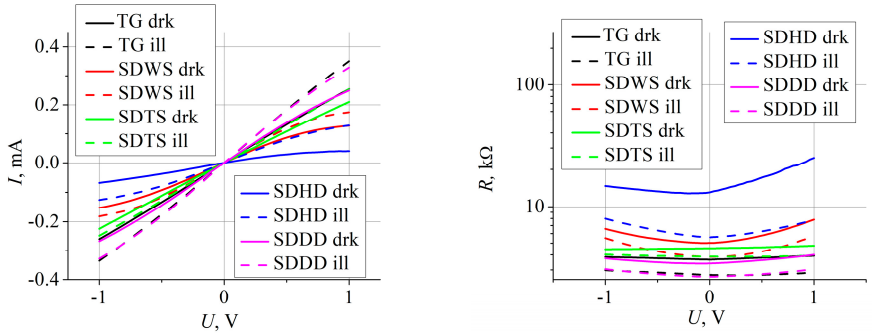


Figure A4. The I-V characteristics of AD1 bow-tie diodes (**a**) and the dependencies of the resistance of the diodes on the applied voltage (**b**) of all studied structures in the dark and under illumination.

References

1. Pozhela, J.K.; Repshas, K.K.; Shilalnikas, V.J. Hot current carriers in Ge and Si. In Proceedings of the International Conference on the Physics of Semiconductors, Exeter, UK, 16–20 July 1962.
2. Harrison, R.I.; Zucker, J. Hot-Carrier Microwave Detector. *Proc. IEEE* **1966**, *54*, 588–595. [CrossRef]
3. Ašmontas, S. *Electrogradient Phenomena in Semiconductors*; Mokslas: Vilnius, Lithuania, 1984; 184p. (In Russian)
4. Sužiedėlis, A.; Gradauskas, J.; Ašmontas, S.; Valušis, G.; Roskos, H.G. Giga- and terahertz frequency band detector based on an asymmetrically-necked n-n^+-GaAs planar structure. *J. Appl. Phys.* **2003**, *93*, 3034–3038. [CrossRef]
5. Minkevičius, L.; Tamošiūnas, V.; Kašalynas, I.; Seliuta, D.; Valušis, G.; Lisauskas, A.; Boppel, S.; Roskos, H.G.; Köhler, K. Terahertz heterodyne imaging with InGaAs-based bow-tie diodes. *Appl. Phys. Lett.* **2011**, *99*, 131101. [CrossRef]
6. Bauer, M.; Venckevičius, R.; Kašalynas, I.; Boppel, S.; Mundt, M.; Minkevičius, L.; Lisauskas, A.; Valušis, G.; Krozer, V.; Roskos, H.G. Antenna-coupled field-effect transistors for multi-spectral terahertz imaging up to 4.25 THz. *Opt. Express* **2014**, *22*, 19250. [CrossRef] [PubMed]
7. Kašalynas, I.; Venckevičius, R.; Valušis, G. Continuous Wave Spectroscopic Terahertz Imaging with InGaAs Bow-Tie Diodes at Room Temperature. *IEEE Sens. J.* **2013**, *13*, 50–54. [CrossRef]
8. Jokubauskis, D.; Minkevičius, L.; Seliuta, D.; Kašalynas, I.; Valušis, G. Terahertz homodyne spectroscopic imaging of concealed low-absorbing objects. *Opt. Eng.* **2019**, *58*, 023104. [CrossRef]
9. Minkevičius, L.; · Tamošiūnas, V.; Kojelis, M.; Žąsinas, E.; ·Bukauskas, V.; · Šetkus, A.; Butkutė, R.; Kašalynas, I.; Valušis, G. Influence of Field Effects on the Performance of InGaAs-Based Terahertz Radiation Detectors. *J. Infrared Millim. Terahertz Waves* **2017**, *38*, 689–707. [CrossRef]
10. Ašmontas, S.; Anbinderis, M.; Čerškus, A.; Gradauskas, J.; Sužiedėlis, A.; Šilėnas, A.; Širmulis, E.; Umansky, V. Gated bow-tie diode for microwave to sub-terahertz detection. *Sensors* **2020**, *20*, 829. [CrossRef] [PubMed]

11. Kašalynas, I.; Venckevičius, R.; Seliuta, D.; Grigelionis, I.; Valušis, G. InGaAs-Based Bow-Tie Diode for spectroscopic terahertz imaging. *J. Appl. Phys.* **2011**, *110*, 114505. [CrossRef]
12. Sužiedėlis, A.; Ašmontas, S.; Gradauskas, J.; Čerškus, A.; Anbinderis, M. Indirect measurement of electron energy relaxation time at room temperature in two dimensional heterostructured semiconductors. *Materials* **2022**, *15*, 3224. [CrossRef] [PubMed]
13. Williams, R. *Processing Methods*, 2nd ed.; Artech Modern GaAs House: Norwood, MA, USA, 1990; 437p.
14. Dienys, V.; Kancleris, Ž.; Martūnas, Z. *Warm Electrons*; Mokslas: Vilnius, Lithuania, 1983; 144p. (In Russian)
15. Sužiedėlis, A.; Ašmontas, S.; Gradauskas, J.; Čerškus, A.; Požela, K.; Anbinderis, M. Competition between Direct Detection Mechanisms in Planar Bow-Tie Microwave Diodes on the Base of InAlAs/InGaAs/InAlAs Heterostructures. *Sensors* **2023**, *23*, 1441. [CrossRef] [PubMed]
16. Berberan-Santos, M.N. A luminescence decay function encompassing the stretched exponential and the compressed hyperbola. *Chem. Phys. Lett.* **2008**, *460*, 146–150. [CrossRef]
17. Berberan-Santos, M.N.; Bodunov, E.N.; Valeur, B. Mathematical functions for the analysis of luminescence decays with underlying distributions: 2. Becquerel (compressed hyperbola) and related decay functions. *Chem. Phys.* **2005**, *317*, 57–62. [CrossRef]
18. Mooney, P.M. Deep donor levels (DX centers) in *III-V* semiconductors. *J. Appl. Phys.* **1990**, *67*, R1–R26. [CrossRef]

Disclaimer/Publisher's Note: The statements, opinions and data contained in all publications are solely those of the individual author(s) and contributor(s) and not of MDPI and/or the editor(s). MDPI and/or the editor(s) disclaim responsibility for any injury to people or property resulting from any ideas, methods, instructions or products referred to in the content.